BULLETIN

OF THE KOREAN CHEMICAL SOCIETY

VOLUME 11, NUMBER 1
FEBRUARY 20, 1990

BKCS 11(1) 1-84
ISSN 0253-2964

Etching of an Al Solid by $SiCl_4$ Molecules at 600 eV

Seung Chul Park†, Chul Hee Cho, and Chang Hwan Rhee**

Department of Chemistry, and Institute of Basic Science, Kangweon National University, Chuncheon 200 - 701. *Received February 16, 1989*

We present a theoretical investigation on the etching of an Al solid by $SiCl_4$ molecules at a collision energy of 600 eV. The classical trajectory method is employed to calculate Al etching yields, degree of anisotropy, kinetic energy distribution and angular distribution. The calculated results are compared with the reaction of a Cu solid by $SiCl_4$. The major products of the reaction are aluminum monomers and dimers together with considerable quantities of multimers. The Al solid shows better etching yield and better anisotropy than the Cu solid. This is consistent with the problem in the CMOS micro-fabrication of the CuAl and CuAlSi alloys. The relevance of these calculations for the dry etching of CuAl alloy is discussed.

Introduction

The study of plasma and reactive ion etching on semiconductor and metal solids has received extensive attention in recent years.[1-20] The main reason for this is that reactive sputter etching is a widely used process in the micro-fabrication of very-large-scale-integration (VLSI) circuits. With the growing importance of radiation induced processing technologies, such as reactive ion plasma etching and laser induced chemical etching and deposition, it has become necessary to understand the mechanisms whereby ions, photons and electrons influence surface chemical reactions.

Experimentally, the etching rates and product distributions of plasma assisted etching have been measured by secondary ion mass spectroscopy, quartz crystal microbalance, and low-energy ion scattering spectrometry and several qualitative and quantitative models of etching processes have been proposed.[5-14] Experimental investigation of dry etching is primarily concerned with measuring the following quantities: the etching yield, y, defined by

$$y = \frac{\text{number of ejected solid atoms}}{\text{number of incident molecules or ions}} \quad (1)$$

the kinetic energy and angular distributions of the sputtered atoms, and elucidation of the sputtering mechanisms. The kinetic energy and angular distributions yield information about the surface structure and the mechanisms of particle ejection. Although there has been a great deal of effort to understand the details of etching mechanisms and dynamics, the available information to describe the details of the mechanisms are quite limited.[4-6] A major difficulty arises from the lack of knowledge of interactions between the plasma, ion and solid. Thus theoretical calculations have an important role in the elucidation of mechanisms. Computer simulations allow the determination of average experimental quantities, which may be compared with direct measurements in the laboratory, but, in addition, by following the motion of each particle in time, they permit physical insight into the microscopic mechanisms that give rise to these phenomena.

Plasma reactions on metal solids are an important class of reactions in the industrial manufacture of VLSI chips.[1-4] Extensive theoretical and experimental studies of plasma reaction on copper solid have been reported[15-31,34] and have proposed details sputtering mechanisms.[32-34] Key reactions on metal etching in CMOS micro-fabrication are the reactions of Cu, Al and Cu-Al alloys with polyatomic gas plasmas such as $SiCl_4$, CCl_4, BCl_3 and mixtures of these gases with Cl_2[2,12]. However, very little detailed experimental investigation of the reaction on Al solids and Cu-Al alloys has been done, and the mechanisms involved are unknown. Hence there is a need for theoretical investigation of these systems.

As a first step toward the reactions of plasma with Al solids and Al-Cu alloys, we investigate the reaction dynamics of the plasma assisted chemical reaction on an aluminum solid using classical trajectory method. A model

† SEC Fellow 1987-1989.

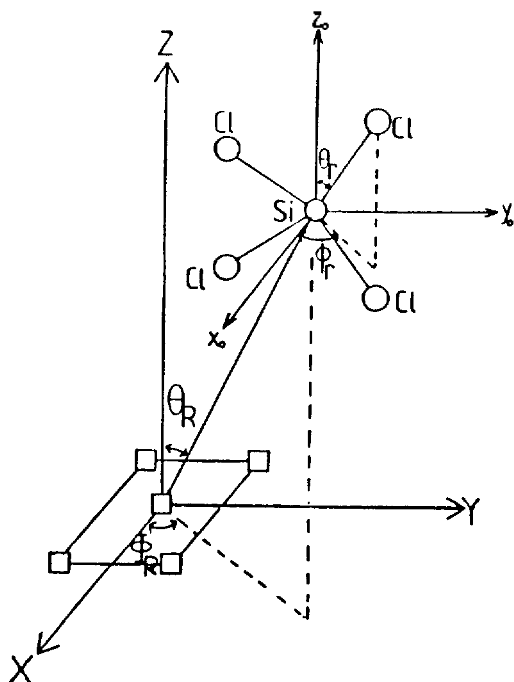

Figure 1. The coordinate system of the $SiCl_4$ + Al(001) system.

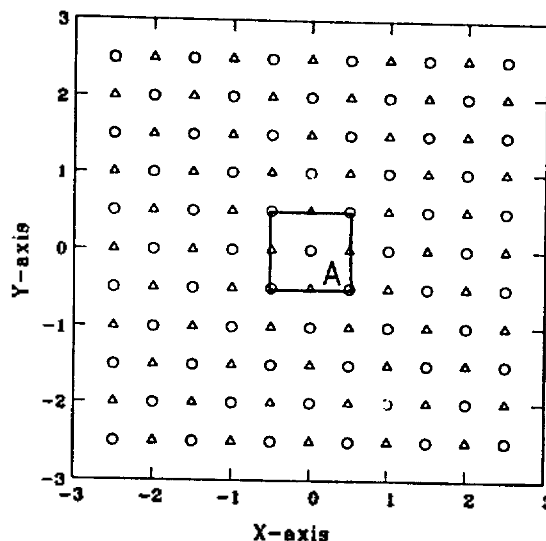

Figure 2. The Al(001) Microcrystallite. The open circles (○), and triangles (△) represent the first and second layer atoms respectively. The third and fourth layer atoms are directly below the first and second layer atoms respectively. The target sites of the $SiCl_4$ molecular beam are sampled on the unit cell area of *A* (solid line).

$SiCl_4$ + Al(001) system is employed to calculate etching yield, the nature of products of the reactions and the energy and angular distributions of the products. The results are compared with the reaction of a copper solid by $SiCl_4$ molecules by Park *et al.*[34] We expect that this comparison could give some information on the difficulties of the etching of Cu solid and the problems of the etching of Al-Cu alloys(≤4%). Those are well known problems in the CMOS micro-fabrication.

In section II, a description of the classical trajectory theory for the $SiCl_4$ + Al(001) is presented. In section III, the construction of the model system and the interaction potentials are discussed. The numerical details of the scattering calculations are described in section IV. Results and discussion are given in section V. Concluding remarks are contained in section VI.

Theory

The approach used here to treat the gas-surface collision dynamics is based on the trajectory method which has been discussed elsewhere[34-38] and we will present only a brief discussion of its application to the reaction of a polyatomic molecule with an aluminum solid as previously Park *et al.*[34] We consider $SiCl_4$ + Al(001) explicitly, although the treatment is quite general.

The coordinate system employed is shown in Figure 1. First, we define a set of coordinates (X, Y, Z) with the Z-axis fixed in space in the [001] direction, and the X and Y axes in the surface plane in the [100] and [010] directions, respectively. The $SiCl_4$ molecules have a set of body-fixed axes (x, y, z) which are determined by the Eckart conditions[39]

The classical Hamiltonian of the system is

$$H=\sum_i \frac{P_i^2}{2m_i}+V(r_i) \tag{2}$$

where i is the index for the Si, Cl and solid Al atoms and $V(r_i)$ is the potential energy surface. We expand $V(r_i)$ as a sum of atom-atom potentials in the form

$$V(r_1,\cdots,r_n)=\sum_{i=1}^{N-1}\sum_{j>i}^{N} V(r_i,r_j). \tag{3}$$

The scattering is described by an ensemble of classical trajectories which are the solutions of Hamilton's equations of motion,

$$\dot{p}_i=-\frac{\partial H}{\partial r_i}, \tag{4}$$

$$\dot{r}_i=\frac{\partial H}{\partial p_i}, \tag{5}$$

where p_i and r_i are the canonically conjugated momenta and positions respectively, for the Si, Cl, and solid Al atoms. The final positions and momenta are saved and analysed as described in section IV to determine ejection yields, energy and angular distributions and product formation.

Interaction Potential

The aluminum lattice is of the face-centered cubic structure.[40] The model microcrystallite used in this simulation consists of 61, 60, 61, and 60 atoms in the first, second third, and fourth layers respectively. The relative disposition of the solid atoms is shown in Figure 2.

The interaction between the solid atoms is described by a pairwise sum of Moliere-Spline-Morse potential functions[23]

$$\begin{aligned} V_{ij}&=Ae^{-Br_{ij}} && 0\le r_{ij}\le R_a \\ V_{ij}&=C_0+C_1r_{ij}+C_2r_{ij}^2+C_3r_{ij}^3 && R_a\le r_{ij}\le R_b \\ V_{ij}&=D(e^{-2\alpha(r_{ij}-r_e)}-2e^{-\alpha(r_{ij}-r_e)}) && R_b\le r_{ij}\le\infty. \end{aligned} \tag{6}$$

The coefficients C_0, C_1, C_2, C_3 are chosen so that V_{ij} is con-

Table 1a. Morse Parameters for Pair Interactions

Pair interactions	D (eV)	(A^{-1})	r_e (A)
Al-Al(solid)[a]	0.423	1.165	2.850
Al-Si[b]	2.34	1.47	2.40
Al-Cl[c]	5.12	1.13	2.13
Si-Cl[d]	3.95	1.46	2.01
Ci-Cl[e]	1.64(-2)	8.29	3.28
Al-Al(gas phase)[f]	1.55	1.40	2.47

[a]From Refs. 42 and 44; r_e from lattice constant in Ref. 40. [b]From Ref. 43. [c]From Ref. 43. [d]From Ref. 45. [e]D estimated from the Cl_2–Cl_2 van der Waal interaction in Ref. 46; from the bending frequency of $SiCl_4$ in Ref. 47; and r_e from the Si–Cl bond length using the tetrahedral geometry of the $SiCl_4$ molecule. [f]From Ref. 43.

Table 1b. Born-Mayer-Spline Parameters for the Al solid

Moliere			Spline			Connection	
A(keV)	B(A^{-1})	C_0(eV/A)	C_1(eV/A)	C_2(eV/A^2)	C_3(eV/A^3)	R (A)	R_b(A)
1.0397	2.7038	21.895	85.439	-91.998	22.128	1.576	2.155

From Ref. 42 and 44.

tinuous up to, and including, the first derivative. Due to computational limitations, we considered only first nearest neighbour interactions in the Al solid.

The interaction between incident $SiCl_4$ molecules and Al solid atoms, and Si-Cl and Cl-Cl interactions in the $SiCl_4$ molecules, are described by the pairwise sum of More potentials which are similar to previously as Park *et al.*[34],

$$V_{ij}=De^{-\alpha(r-r_e)}\left[e^{-\alpha(r-r_e)}-2\right], \tag{7}$$

where i, j indicate the index of the $SiCl_4$ and the aluminum solid atoms. All the potenial parameters are shown in Table 1. In constructing the interaction potentials, we have not taken into account the local relaxation of the surface or surface reconstruction.

Numerical Details

Initial Conditions. The trajectory calculations were performed in the usual manner.[34-38] The solid atoms are initially at their equilibrium positions with no velocity. The initial conditions of the $SiCl_4$ molecules are determined from the orientations of the molecular beam (Θ_R, Φ_R) with beam kinetic energy, E_{init}, and the orientations of molecule, (θ_r, ϕ_r). The atoms in the $SiCl_4$ molecules are initially at their equilibrium separations. The initial position vectors of the jth atom, $(j=1,\cdots,5)$, in the $SiCl_4$ are denoted as (x_o^j, y_o^j, z_o^j) with respect to the space-fixed axis system (x_o, y_o, z_o) of Figure 1. The Si atom is at the origin of the body-fixed coordinate system, while one of the Cl atoms is located on the z axis, and another in the xz plane. The spherical polar and azimuthal angles (θ_r, ϕ_r) give the orientation of the space-fixed axes with respect to the body-fixed axes and are selected using phase space sampling according to,

$$\begin{aligned}\theta_r&=\cos^{-1}(1-\xi)\\ \phi_r&=2\pi\xi\end{aligned} \tag{8}$$

where ξ is the uniform random number between 0 and 1. The zero point energy of the molecular vibration is not considered. The position vectors of the $SiCl_4$ molecules with the internal orientations, (θ_r, ϕ_r) in the space-fixed coordinates are then

$$\begin{pmatrix} x_o^j \\ y_o^j \\ z_o^j \end{pmatrix} = \mathbf{R}_1(\theta_r)\mathbf{R}_2(\phi_r)\begin{pmatrix} x^j \\ y^j \\ z^j \end{pmatrix} \tag{9}$$

where $\mathbf{R}_1(\theta_r)$ and $\mathbf{R}_2(\phi_r)$ are the rotation matrices[41]

$$\mathbf{R}_1(\theta_r)=\begin{pmatrix} 1 & 0 & 0 \\ 0 & \cos\theta_r & \sin\theta_r \\ 0 & -\sin\theta_r & \cos\theta_r \end{pmatrix} \tag{10}$$

and

$$\mathbf{R}_2(\phi_r)=\begin{pmatrix} \cos\phi_r & \sin\phi_r & 0 \\ -\sin\phi_r & \cos\phi_r & 0 \\ 0 & 0 & 1 \end{pmatrix} \tag{11}$$

Then the initial conditions of the $SiCl_4$ molecules in the space-fixed coordinates of the system are

$$P_{x_{init}}^j=\sqrt{2m_jE_{init}}\sin\Theta_R\cos\Phi_R, \tag{12}$$

$$P_{Y_{init}}^j=\sqrt{2m_jE_{init}}\sin\Theta_R\sin\Phi_R, \tag{13}$$

$$P_{Z_{init}}^j=\sqrt{2m_jE_{init}}\cos\Theta_R. \tag{14}$$

$$Z_{init}^j=Z_o^j+C:\text{ large and positive}, \tag{15}$$

$$X_{init}^j=X_o^j+\bar{X}+(P_{x_{init}}^j/P_{z_{init}}^j)Z_{init}^j, \tag{16}$$

$$Y_{init}^j=Y_o^j+Y+(P_{Y_{init}}^j/P_{Z_{init}}^j)Z_{init}^j, \tag{17}$$

where $(\bar{X}, \bar{Y})$ is the target site for the $SiCl_4$ molecular beam on the solid, and j is the index for the jth atom in the $SiCl_4$ molecule. The target site coordinates were sampled on a 1×1 unit cell of the solid surface by a uniform random number.

Etching Yield and Degree of Anisotropy. Trajectories are calculated by the integration of the three dimensional classical mechanical equations of motion for $SiCl_4$ molecules, and the aluminum solid atoms. The trajectories are terminated when the most energetic particle remaining in the crystal has 2 eV of kinetic energy. This is the same method as that used by Garrison *et al.*[23] The ejected atoms are tested in the following ways. First, if the Z-component of the position of an atom has a value of more than 1 A with a positive Z-component of momentum, then we calculate the kinetic and potential energies, T_{atom}, V_{atom} respectively. When the total energy $E_{atom}=T_{atom}+V_{atom}$, is positive, the atom is considered to be ejected from the surface. The etching yield Y is as in equation (1). Our method for determining if an atom has been ejected is the same as that due to Garrison *et al.*[23] except that we put the extra condition on the Z-component displacement. Our method to test the formation of products is similar to the one that has been used to check for the multimer formation by Garrison *et al.*[23,30,31] A typical 100 trajectories are propagated on the unit cell of the aluminum surface with beam kinetic energies, E_i, at 600 eV and beam orientations $\Theta_R=0$ deg, $\Phi_R=0$ deg which are similar condition of the plasma etching in the CMOS micro-fabrication.

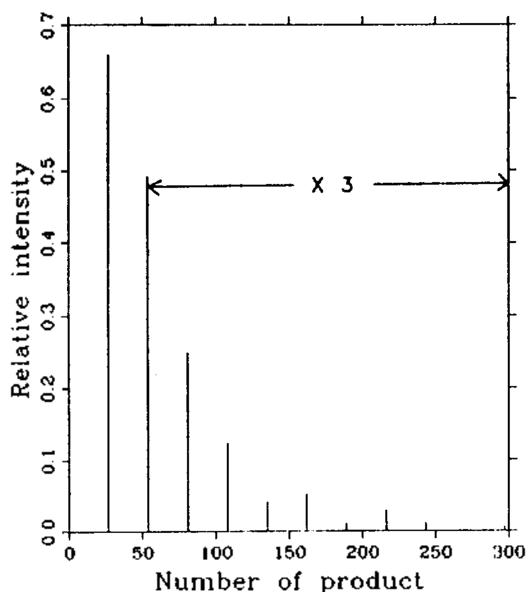

Figure 3. Product distribution for the reaction of Al(001) + $SiCl_4$ for the initial beam kinetic energy 600 eV. Relative intensity *vs* mass number of product (amu) are plotted.

The final results are an ensemble average of the trajectories.

The degree of anisotropy defined by Mogab[2] is,

$$A_f = 1 - \frac{v_l}{v_v}, \tag{18}$$

where v_l and v_v are the lateral and vertical etch rates respectively. We assume that the rate of etching is proportional to the momentum transfer, then

$$v_l \propto <\delta P_l> \\ v_v \propto <\delta P_v> \tag{19}$$

and

$$A_f = 1 - \frac{v_l}{v_v} \approx 1 - \frac{<\delta P_l>}{<\delta P_v>}. \tag{20}$$

where ··· indicates an ensemble average.

Results and Discussion

First, we have calculated the product distribution of the etching of the aluminum solid by $SiCl_4$ molecules which is shown in the Figure 3.

The major products of the reaction are aluminum monomers and dimers together with considerable amounts of multimers as shown in the Figure 3. No chlorine compounds are ejected in the calculations. These results are quite different from those of the reaction of the copper solid by $SiCl_4$ molecules by Park *et al.*[34] In the reaction of the copper solid, the major products are atomic Cu together with trace quantities of copper multimers. Although they did not detect chlorine compounds in the reactions, the CuCl and $CuCl_2$ molecules were detected intact on the surface. In the reaction of the Al solid on the other hand the AlCl, $AlCl_2$ and $AlCl_3$ are not detected even on the surface of the Al solid. We have found that all the chlorine atoms penetrate few layer of the Al solid. This means that the reaction mechanisms of the Cu and the

Table 2. Calculated Etching Yields, Mean Kinetic Energy and Degree of Anistropy

Reaction system	y	K.E. /eV	A_f
$SiCl_4$ + Al(001)	9.32	5.13	−0.044
$SiCl_4$ + Cu(001)	8.72	6.05	−0.230

Al solids with $SiCl_4$ molecules are quite different. In the reaction of the Cu solid, the chlorine atoms are dissociated from the $SiCl_4$ molecules and react with Cu atoms on the Cu solid which remain intact on the Cu solid. In the reaction of the Al solid, the chlorine atoms are dissociated and penetrate into the Al layers. This can be easily understood with the structures and the interaction potentials of the Cu and the Al solid. The nearest nighbour distances of the Cu and the Al solids are 2.556 Å and 2.850 Å respectively, and the interaction of the Cu-Cu atoms in the Cu solid is stronger than that of the Al atoms in the Al solid. This is consistent with the problem[2,12] in VLSI micro-fabrication where the sputtering of CuAl and CuAlSi alloys gives rise to involatile copper chloride residues forming on the surface when the copper concentration is high (e.g.>4%).

We also have calculated the degree of anisotropy, A_f for the reaction of the Al solid by $SiCl_4$ molecules and have compared with that of the Cu solid which are shown in the Table 2.

Neither of these systems give good anisotropic sputter etching according to the definition of Mogab.[2] However, the anisotropy of the reaction of the Al solid is relatively better than that of the reaction of the Cu solid. This is also consistent with the problem[2,12] in the CMOS micro-fabrication of the CuAl and the CuAlSi alloys where the degrees of anisotropy are getting worse with increasing concentration of the copper atoms. This may be due to that the residues of the CuCl and $CuCl_2$ scatter the ejected Cu atoms to parallel direction in the reaction of the Cu solid. On the other hand the Al atoms can be ejected more freely to the perpendicular direction than that of the reaction of the Cu solid, since there is no residues in the reaction of the Al solid.

The calculated etching yield of the Al solid is 9.32 which is greater than that of the Cu solid, 8.72 as we expected. The lower value of the Cu etching yield is also due to the residues of the CuCl and $CuCl_2$ which reflect the ejecting Cu atoms from the inner layer by indirect collision back to the inner layer direction. On the other hand the Al atoms can be ejected freely without residues from the inner layers by radiation damage.

The kinetic energy distribution of ejected Al atoms is shown in the Figure 4 together with the reaction of the Cu solid. The solid histogram represents the result of this study and the dashed one is for the Maxwell-Boltzmann distribution obtained at the temperature which has been calculated based on data of the average kinetic energy of ejected atoms in this study. As seen in this figure, the shape of the energy distribution of the ejected atoms resembles the Maxwell-Boltzmann distribution curve (Al fit better than Cu relatively) as were the cases of the other systems both in experiment[5,48] and theoretical calculations.[25,26,34,35] It is difficult to define surface temperature accurately of these cases. However, since the peak of the Al atoms is wider of the two and the

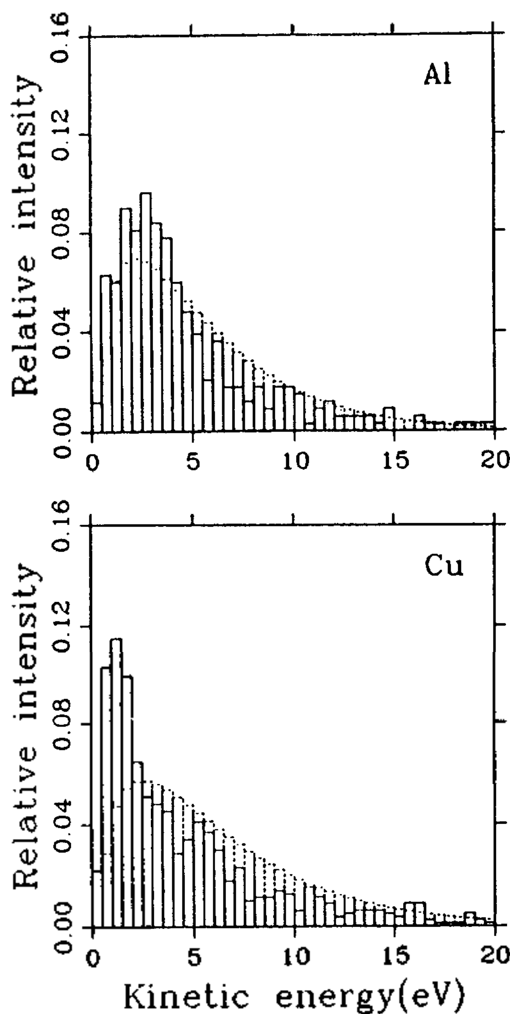

Figure 4. Histogram of the kinetic energy distribution of ejected aluminum atoms for the initial beam kinetic energy 600 eV. The solid histogram represents the result of this study and the dashed one is for the Maxwell-Boltzmann distribution. Bin size is 0.5 eV.

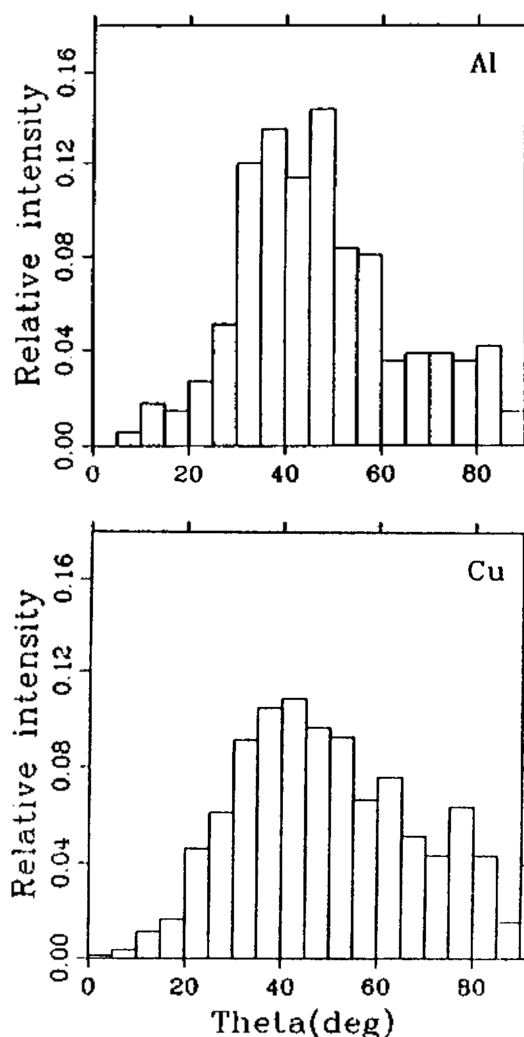

Figure 5. Histogram of the polar angle distribution of ejected aluminum atoms for the initial beam kinetic energy 600 eV. Bin size is 5°.

maximum kinetic energy of Al atoms (around 3.0 eV) is higher than that of the Cu atoms (around 1.5 eV), it is indicated that the surface temperature of the Al solid is significantly higher than that of the Cu solid. This hotter surface of the Al solid may be due to the fact that the excitation is easier for the weaker and longer Al-Al bond, which in turn could produce the more violently moving free Al atoms in the solid than the case for the tighter and shorter Cu-Cu bond. The reason for the better fit of the energy distribution of the ejected Al atoms into the Maxwell-Boltzmann distribution curve is that the possibility for the Al solid tends to reach the thermal equilibrium during the reactions is increased may due to the existence of penetrated chlorine atoms in inner layers of the Al solid. When the dissociated chlorine atoms penetrate into layers of the Al solid, those chlorine atoms cause the radiation damage in the layer and the resulting ejection of atoms could take place. However, in the case of the Cu solid, the possibility of this radiation damage is relatively lower than the Al solid, because of lower penentration of chlorine atoms. The majority of the ejected Cu atoms come from the direct collision process. Since the direct collision produces the more energetic free atoms than the indirect process (the radiation damage), the reason for the higher average kinetic energy of the ejected Cu atoms (6.05 eV for Cu and 5.12 eV for Al) while the most probable kinetic energy is higher for the Al atoms as seen in Figure 4, could be explained. And the sudden, non-adiabatic ejection of the Cu atoms with little or no coupling to the rest of the solid might have caused the steeper rise and faster decay in the energy distribution curve of the Cu atoms and the resulting deviation from the Maxwell-Boltzmann distribution curve.

Figures 5 and 6 show the polar and azimuthal angular distributions of the ejected atoms by $SiCl_4$ molecules. The distribution of the polar angle is quite broad with maximum around 45°. These polar angular distributions indicate that large amounts of parallel momentum are being transferred to the ejected atoms during collision processes. In the distribution of the Al solid, the ejected Al atoms at angles less than 45° are more than that of atoms with angles greater than 45°. However, the distribution of the Cu solid is quite the opposite. This is consistent with the fact that the anisotropy of the reaction of the Al solid is better than that of the Cu solid. The distributions of the azimuthal angle are, by contrast, quite structured with sharp maxima and minima. The loca-

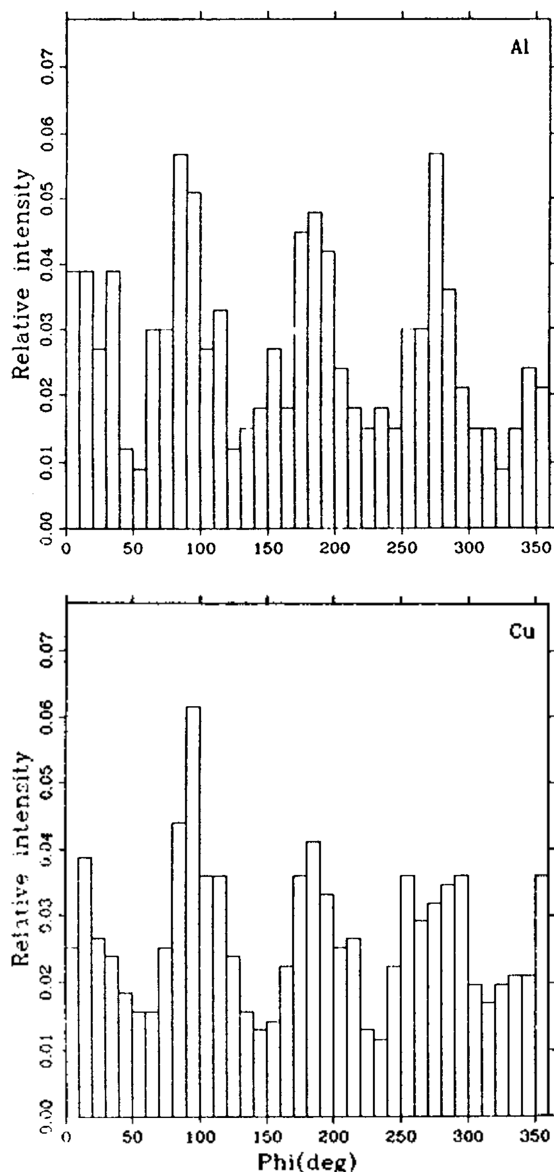

Figure 6. Histogram of the azimuthal angle distribution of ejected aluminum atoms for the initial beam kinetic energy 600 eV. Bin size is 5°.

tions of the maxima and minima on the azimuthal angular distributions are related to the symmetry directions of the Al and the Cu solids. Overall shapes of the distributions for the two solids are quite similar. Those are due to same symmetry properties of both solids in the fcc structure. The four maxima at 90°, 180°, 270° and 360° arise from the ejected atoms preferentially ejecting in the direction of the fourfold holes surrounding them.[20] Similarly, the minima at 45°, 135°, 225° and 315° arise correspond to the four nearest neighbours in the first layer. Similar symmetry-related angular distributions have been reported in calculations by Garrison and coworkers[22,24,26] and have been observed experimentally by various groups.[49,50]

Summary

The classical trajectory method has been applied to perform computer simulation on the sputter etching of an Al solid at a collision energy of 600 eV. Etching yield, degree of anisotropy, kinetic energy distribution and angular distribution have been calculated. The calculated results are compared to those of the Cu system.[34] The Al solid shows better etching yield and better anisotropy than that of the Cu system. The major products of the reaction of the Al solid are aluminum monomers, dimers and considerable amounts of multimers, a result which is quite different from those of the Cu solid. These indicate that the reaction mechanisms of those systems are quite different. The following is the major differences in both systems. In the Al system, the dissociated chlorine atoms penetrate into the inner layers which cause radiation damage to the Al solid while in the Cu system the dissociated chlorine atoms react with Cu atoms and form involatile residues, CuCl and $CuCl_2$ which remain intact on the surface. These residues cause a lower etching yield and higher anisotropy in the case of the Cu solid. These are consistent with the problem[2,12] in the CMOS micro-fabrication of the CuAl and CuAlSi alloys. The collision energy dependence of the etching of the Al solid as well as more details of physical discussion on reaction mechanisms are currently in progress in our group and will be reported separately elsewhere soon.

Acknowledgements. This work was supported by grant from ASAN Foundation. Numerical calculations were performed on the IBM 3083 system at KAIST, SERI and the CYBER 170-720 system at Kangweon National University. One of us (S.C. Park) would like to thank KAIST, SERI for the SEC fellowship to the basic science research. We are pleased to acknowledge useful comments from the referees which brought us to see new insight of this work.

References

1. S. M. Sze, *in VLSI Technology*, edited by S. M. Sze, pp. 1-7 (McGraw-Hill, New York, 1983).
2. C. J. Mogab, *in VLSI Technology*, edited by S. M. Sze, pp. 303-346 (McGraw-Hill, New York, 1983).
3. B. N. Chapman, *Glow Discharge process*, (Wiley, New York, 1980).
4. J. W. Coburn and H. F. Winters, *Ann. Rev. Mater. Sci.* **13**, 91 (1983).
5. J. W. Coburn and H. F. Winters, *J. Appl. Phys.* **50**, 3189 (1979).
6. J. W. Coburn, E.-A. Knabbe, and E. Kay, *J. Vac. Sci. Technol.* **20**, 480 (1982).
7. E. L. Barish, D. J. Vitkavage, and T. M. Mayer, *J. Appl. Phys.* **57**, 1336 (1985).
8. V. M. Donnelly, D. L. Flamm, W. C. Dautremont-Smith, and D. J. Werder, *J. Appl. Phys.* **55**, 242 (1984).
9. A. W. Kolfschoten, R. A. Haring, A. Haring and A. E. de Vries, *J. Appl. Phys.* **55**, 3813 (1984).
10. D. J. Oostra, A. Haring, R. P. van Ingen, and A. E. de Vries, *J. Appl. Phys.* **64**, 315 (1988).
11. T. I. Cox and V. G. I. Deshmukh, *Appl. Phys. Lett.* **47**, 378 (1985).
12. W. Y. Lee and J. M. Eldridge, *J. Appl. Phys.* **55**, 3813 (1984).
13. K. Miyake, S. Tachi, K. Yagi, and T. Tokuyama, *J. Appl. Phys.* **53**, 3214 (1982).

14. Ch. Steinbruchel, *J. Vac. Sci. Technol.* **B2**, 38 (1984).
15. S. P. Holland, B. J. Garrison, and N. Winograd, *Phys. Rev. Lett.* **43**, 220 (1979).
16. J. B. Gibson, A. N. Goland, M. Milgram, and G. H. Vineyard, *Phys. Rev.* **120**, 1229 (1960).
17. D. E. Harrison, Jr., N. S. Levy, J. P. Johnson, III and H. M. Effron, *J. Appl. Phys.* **39**, 3742 (1968).
18. M. T. Robinson, *J. Appl. Phys.* **40**, 2670 (1969).
19. D. E. Harrison, Jr., *J. Appl. Phys.* **40**, 3870 (1969).
20. D. E. Harrison, Jr., W. L. Moore, Jr., and H. T. Holcombe, *Radiation Effects* **17**, 167 (1973).
21. D. P. Jackson, *Can. J. Phys.* **53**, 1513 (1975).
22. N. Winograd, B. J. Garrison, and D. E. Harrison, Jr., *Phys. Rev. Lett.* **41**, 1120 (1978).
23. B. J. Garrison, N. Winograd, and D. E. Harrison, Jr. *Phys. Rev. B* **18**, 6000 (1978).
24. S. P. Holland, B. J. Garrison, and N. Winograd, *Phys. Rev. Lett.* **44**, 756 (1980).
25. B. J. Garrison, N. Winograd, and D. E. Harrison, Jr., *Surf. Sci.* **87**, 101 (1979).
26. K. E. Foley and B. J. Garrison, *J. Chem. Phys.* **72**, 1018 (1980).
27. R. A. Gibbs, S. P. Holland, K. E. Foley, B. J. Garrison, and N. Winograd, *J. Chem. Phys.* **76**, 684 (1982).
28. B. J. Garrison, *J. Am. Chem. Sco.* **104**, 6211 (1982).
29. K. E. Foley, N. Winograd, B. J. Garrison, and D. E. Harrison, Jr., *J. Chem. Phys.* **80**, 5254 (1984).
30. D. W. Moon, N. Winograd, and B. J. Garrison, *Chem. Phys. Lett.* **114**, 237 (1985).
31. B. J. Garrison, in Potential Energy Surfaces and Dynamics Calculations for Chemical Reactions and Molecular Energy Transfer, Chapter 36, edited by D. G. Truhlar, (Plenum Press, New York, 1981).
32. P. Sigmund, *Phys. Rev.* **184**, 383 (1969).
33. P. Sigmund, in Topics in Applied Physics, edited by R. Behrisch, Vol. 47, pp. 10–71, (Springer-Verlag, Heidelberg, 1981).
34. S. C. Park, R. A. Stansfield, and D. C. Clary, *J. Phys. D.* **20**, 880 (1987).
35. S. C. Park and D. C. Clary, *J. Appl. Phys.* **60**, 1183 (1986).
36. J. M. Bowman and S. C. Park, *J. Chem. Phys.* **77**, 5441 (1982).
37. S. C. Park and J. M. Bowman, *J. Chem. Phys.* **81**, 6277 (1984).
38. R. R. Lucchese and J. C. Tully, *Surf. Sci.* **137**, 570 (1983).
39. S. Califano, *Vibrational States*, (Wiley, New York, 1976).
40. R. W. G. Wyckoff, Ed., *Crystal Structures table III*, 10, Interscience Publishers Inc., New York (1960).
41. H. Goldstein, *Classical Mechanics*, (Addison-Wesley, Reading, Mass. 1950).
42. J. J. Burton and G. Jura, *J. Chem. Phys.* **71**, 1937 (1967).
43. K. P. Huber and G. Herzberg, *Constants of Diatomic Molecules*, (Van Nostrand Reinhold Company, New York, 1979).
44. J. B. Gibson, A. N. Goland, M. Milgram, and G. H. Vineyard, *Phys. Rev.* **120**, 1229 (1960).
45. E. A. V. Ebsworth, *Volatile Silicon Compounds*, (Pergamon Press, Oxford 1963).
46. S. L. Price and A. J. Stone, *Mol. Phys.* **47**, 1457 (1982).
47. G. Herzberg, *Molecular Spectra and Molecular Structure*, Vol. 2, *Infrared and Raman Spectra of Polyatomic Molecules*, (Van Nostrand Reinhold Company, New York, 1945).
48. B. M. Farmery and M. W. Thompson, *Phil. Mag.* **18**, 415 (1968).
49. A. L. Southern, W. R. Willis, and M. T. Robinson, *J. Appl. Phys.* **34**, 153 (1963).
50. R. S. Nelson and M. T. Thompson, *Proc. R. Soc.* **A 259**, 459 (1961).

Synthesis of 4,5,6,7-Tetraphenyl-8-(substituted)-3(2H)-phthalazinone Derivatives Likely to Posses Antihypertensive Activity

F.A. Yassin, B.E. Bayoumy*, and A.F. El-Farargy

Zagazig University, Faculty of Science Department of Chemistry, Zagazig, Egypt. *Received July 24, 1989*

The interaction of tetraphenylphthalic anhydride with *o*-chlorotoluene under Friedel-Craft condition gives 2-(4-chloro-3-methyl)benzoyl-3,4,5,6-tetraphenyl benzoic acid(1), which on reaction with hydrazine derivatives gave phthalazinones (2a-d). The behaviour of (2a) towards carbon electrophiles and carbon nucleophiles has been investigated. The chlorophthalazinones (4a) also has been synthesised from the action of $PCl_5/POCl_3$ on (2a). The behaviour of (4a) towards nitrogen, and oxygen nucleophiles also have been described.

Introductions

Recently[1,2], 3 (2H)-phthalazinones have been described as being useful as remedies for artroisosclerosis and thromosis, and have also been useful as antihypertensive materials. This promoted us to synthesis some new phthalazinones.

Thus, interaction of tetraphenylphthalic anhydride with *o*-chlorotoluene under Friedel-Craft condition gives 2-(4-chloro-3-methyl)benzoyl-3,4,5,6-tetraphenyl benzoic acid